Published in final edited form as:
Biomaterials. 2011 April ; 32(10): 2540–2545. doi:10.1016/j.biomaterials.2010.12.031.

Enhancement of cell recognition *in vitro* by dual-ligand cancer targeting gold naoparticles

Xi Li[a], **Hongyu Zhou**[a], **Lei Yang**[a], **Guoqing Du**[a], **Atmaram Pai-Panandiker**[b], **Xuefei Huang**[c], and **Bing Yan**[a,d,*]

[a] Department of Chemical Biology and Therapeutics, St. Jude Children's Research Hospital, Memphis, Tennessee, 38105 USA

[b] Department of Radiology, St. Jude Children's Research Hospital, Memphis, Tennessee, 38105 USA

[c] Department of Chemistry, Michigan State University, East Lansing, MI 48824-1322, USA

[d] School of Chemistry and Chemical Engineering, Shandong University, Jinan, 250100, China

Abstract

A dual-ligand gold nanoparticle (DLGNP) was designed and synthesized to explore the therapeutic benefits of multivalent interactions between gold nanoparticles (GNPs) and cancer cells. DLGNP was tested on human epidermal cancer cells (KB), which had high expression of folate receptor. The cellular uptake of DLGNP was increased by 3.9 and 12.7 folds compared with GNP-folate or GNP-glucose. The enhanced cell recognition was due to multivalent interactions between both ligands on GNPs and cancer cells as shown by the ligand competition experiments. Furthermore, the multivalent interactions increased contrast between cells with high and low expression of folate receptors. The enhanced cell recognition enabled DLGNP to kill KB cells under X-ray irradiation at a dose that was safe to folate receptor low-expression (such as normal) cells. Thus DLGP has the potential to be a cancer-specific nano-theranostic agent.

1. Introduction

Cancer remains a major threat to public health. Almost 60% of cancer patients are candidates for radiation therapy during the course of their disease management. The primary mechanism of radiation-induced cell killing is via production of free radicals, which causes the death of cancer cells by disrupting cellular DNA. However, because ionizing radiation does not discriminate malignant and normal cells, radio-toxicity to healthy tissues is a dose-limiting factor [1–3]. Compounds containing elements with a high atomic number (Z), such as iodine (Z=53), can act as radio-sensitizers because of their high mass energy absorption coefficients [4,5]. The higher linear energy transfer and photoelectric interaction products (photoelectrons, Auger electrons and their secondary particles of lower energy through energy loss processes) are hypothesized to enhance the amount of radiation absorbed by cells and tissues containing the radio-sensitizers. Unfortunately, iodine radio-sensitizers are not selective for cancer cells. Furthermore, they may induce hypersensitivity, anaphylactic shock and kidney failure, selective iodide uptake within the thyroid gland and associated

*To whom correspondence should be addressed, bing.yan@stjude.org.

toxicity [6–9]. The relative effect of gold nanoparticles (GNPs, Z=79) is ~3 times that of iodine-containing compounds and ~1217 times that of soft tissue [10,11]. However, GNPs without cancer-targeting function can also enhance the damage to normal tissues due to their accumulation in normal tissues [12–14].

To overcome this obstacle, cancer-targeting molecules, such as antibody [15,16], nucleic acid aptamer [17–19], oligopeptide [20,21], and small targeting molecule [22,23], have been attached to surface of GNPs to enhance cancer cell targeting. Folic acid is one of such small targeting molecules which target the folate receptor (FR) that is over-expressed in ovarian, brain, head and neck, renal, and breast cancers [24–26]. Mediated by the binding between targeting molecules on GNPs and the receptors on the surface of cancer cells, GNPs can be taken up by cancer cells selectively. However, most commonly targeted receptors such as FR, are not only expressed on cancer cells but also on some normal cells, which will cause unintended uptake in these non-targeting cells [10,27]. Nonspecific binding and specific binding to non-targeting cells diminished the effectiveness of targeting molecules [28]. Alternatively, cancer cells typically over-express multiple surface receptors. Based on this fact, dual-ligand targeting approach has been used to enhance the cancer targeting specificity. Efforts have been made to target FR/epidermal growth factor receptor (EGFR) [29], transferring receptor/glucose transporter [30], and $\alpha_v\beta_3$ intergrin/galectin-1 receptor [31]. However, these approaches contain at least one oligopeptide or antibody as targeting ligand, which is usually expensive and suffers from short shelf life. So it's necessary to develop small molecule-based dual-ligand targeting nanocarriers. Here we reported a dual-ligand cancer targeting GNP that could enhance the contrast between FR over-expressing cancer cells and FR low-expressing cells and also generate a significant enhancement of X-ray induced cancer cell death at a dose safe to normal cells.

2. Materials and methods

All chemical reagents were purchased from Sigma-Aldrich (St. Louis, MO) and used without further purification. The synthesis and characterization of Thioctic-PEG-FA (**TA-FA**) and Thioctic-FITC (**TA-FITC**) were listed in Supporting Information. Transmission electron microscope (TEM) images of GNPs were obtained using a JEOL 1200 EX transmission electron microscope (JEOL, Tokyo, Japan) at 80 KV. The images were acquired using an AMT 2k CCD Camera. The UV-Vis absorption spectra of GNPs were carried out with a Varian 5000 UV-Vis spectrometry (Varian, Santa Clara, CA). All the spectra were subtracted background with baseline correction by the absorption of deionized water. Dynamic diameter of GNPs was measured using Dynapro Titan system (Wyatt Technology, Santa Barbara, CA). Flow cytometry analyses were performed on a Guava EasyCyte Mini flow cytometry system (Millipore, Billerica, MA). The Confocal fluorescence microscopy (CFM) images were recorded by a confocal microscopy using a Nikon C1si confocal laser scanning module attached to a motorized Nikon TE2000-E inverted microscope (Nikon Instruments Inc., NY)

2.1 Synthesis of gold nanoparticles

2.1.1 Synthesis of GNP-FA and GNP-glucose (GNP-Glu)—The synthesis procedures for **GNP-FA** and **GNP-Glu** are similar. In a typical experiment for synthesis of **GNP-FA**, 1.5 mL of water containing chloroauric acid (25.0 mg, 0.063 mmol) was added to a solution of **TA-FA** (21.4 mg, 0.032 mmol) in MeOH (12.0 mL). After stirring for 30 min at room temperature, $NaBH_4$ (9.5 mg, 0.252 mmol) in 12 mL water was added to the mixture dropwise. The solution turned red immediately and the solution was stirred for 4 h at room temperature. 1N HCl was added to the reaction mixture dropwise to neutralize the excess $NaBH_4$. To remove the free ligands and solvent from the GNPs, the reaction mixture

was centrifuged at 13000 rpm for 30 min. The colorless supernatant was decanted and the solid was dissolved in 20 mL methanol and deionized water alternatively followed by sonication and centrifugation. This wash-centrifugation cycle was repeated 5 times. After the final washing step, the functionalized GNPs were dried in vacuum at 50 C for 12 h. The GNPs was dissolved in 10 mL phosphate buffered saline (PBS) and was used as stock solution. The gold concentration was determined by inductively coupled plasma mass spectrometry (ICP-MS).

2.1.2 Synthesis of FA-GNP-Glucose (GNP-FA-Glu)—1.5 mL of water containing chloroauric acid (25.0 mg, 0.063 mmol) was added to a solution of **TA-FA** (21.4 mg, 0.032 mmol) and **Thio-Glucose** sodium salt (7.0 mg, 0.032 mmol) in MeOH (12.0 mL). After stirring for 30 min at room temperature, $NaBH_4$ (9.5 mg, 0.252 mmol) in 12 mL water was added to the mixture drop wise. The solution turned red immediately and the solution was stirred for 4 h at room temperature. 1N HCl was added to the reaction mixture drop wise to neutralize the excess $NaBH_4$. The process for purification is same as above.

2.1.3 Synthesis of fluorescent GNP-FA, GNP-Glu and GNP-FA-Glu—1.0 mg **TA-FITC** was added to the corresponding MeOH solution of compound(s) for the synthesis of fluorescent GNPs. The synthesis and purification process is the same as above.

2.2 Cell culture

Human epidermal KB cells were grown in folate-free RPMI-1640 medium (Invitrogen, IL). A549 cells were grown in RPMI 1640 medium. Each cell culture medium was supplemented with 10%fetal bovine serum (FBS), 10 U/mL penicillin and 10 mg/mL streptomycin. Cultures were maintained at 37 °C under a humidified condition with 5% CO_2.

2.3 ICP-MS

KB and A549 cells were cultured in 12-well plate with a density of 20, 000 cells/well. After 24 h of plating, the cells were washed once with cold PBS, and the solutions of nanoparticles were added with a specified final gold concentration. The cells were incubated with GNPs for specified time and washed 3 times with cold PBS to remove extra GNPs. The cells were detached by trypsin-EDTA solution (0.25 % trypsin, 1 mM EDTA). The detached cells were counted and then prepared for ICP-MS.

All ICP-MS measurements were performed on a Varian 820-MS spectrometer (Varain, Santa Clara, CA). After detaching and counting of the cells, 180 μL of resulting cell lysate was digested for 4 h at 37 °C by adding 300 μL aqua regia. 50 μL of the above solution was diluted to 5.0 mL with a 50 ppb ^{236}Y internal standard solution in 1.0% HNO_3 and used for ICP-MS measurements. Cellular uptake experiments with each GNP were repeated 3 times, and each replicate was measured 5 times by ICP-MS. A series of gold standard solutions (1000, 500, 100, 50, 10, 5, and 1 ppb) with 50 ppb ^{236}Y internal standard were prepared before each measurement. The resulting calibration curve was used to calculate the gold concentration taken up by different cells. Two injections of 2.0% HNO_3 solution containing 50 ppb ^{236}Y internal standard were used to wash the instrument between analyses to remove the trace amount of gold.

2.4 X-ray irradiation

KB and A549 cells were cultured in 96-well plate with a density of 5, 000 cells/well. After 24 h of plating, the cells were washed once with cold PBS, and the GNP solutions were added with a specified final gold concentration. The cells were incubated with GNPs for 2 h and then washed 3 times with cold PBS to remove extra GNPs. 100 μL of fresh medium was then added to the plate. The AXR Minishot 160 X-ray cabinet irradiator working at 100 kV

and 3 mA, yielding a mean dose rate of 146.0 R/min was used. The cells were exposed to X-ray irradiation with a total dose of 10 Gy, corresponding to irradiation time of 410 s at dose rate 146 R/min. The XTT measurements were performed 48 h after X-ray irradiation. For all experiments, a copy of 96-well plate with the same cell and without GNPs or X-ray irradiation was used as control.

2.5 Cytotoxicity assay

Cell proliferation kit II (XTT, Roche Diagnostics Corporation, Indianapolis, IN) was used to evaluate the viability of cells after uptake of GNPs and X-ray irradiations. The assay was based on the cleavage of the water soluble yellow tetrazolium salt XTT to form an orange formazan dye by metabolic active cells. The formazan was directly quantified using a Microplate reader, which was correlated with the number of viable cells. Suspension medium was removed 48 h after the X-ray irradiation and 50 μL XTT solutions (1 mg/ml, Sigma) and 100 μL fresh medium were added to each well and incubated at 37 °C for 4 h. The absorbance of all samples was measured at 480 nm and 650 nm separately using a SpectraMax M5 microplate reader (Molecular Devices Sunnyvale, CA) and the cell viability was calculated following the standard procedure. Each experiment was performed three times.

3. Results and discussion

3.1 Design and synthesis of GNPs

To test the dual-ligand targeting hypothesis, we first synthesized **GNP-FA**, **GNP-Glu** and **GNP-FA-Glu** (Figure 1). **GNP-FA** and **GNP-Glu** were synthesized by reduction of chloroauric acid in the presence of $NaBH_4$ and **TA-FA** or **thio-glucose. GNP-FA-Glu** was synthesized by reduction of chloroauric acid in the presence of $NaBH_4$ and both ligands in 1:1 ratio. All GNPs were purified by centrifugation and washed by methanol and water alternatively for 5 times. GNPs were characterized by TEM, dynamic light scattering (DLS), and UV-Vis spectroscopy. The existence of **FA** on dual-ligand GNPs (DLGNPs) were confirmed by UV spectra (Figure 2a). **GNP-FA-Glu** showed characteristic peak at ~520 nm for GNPs and 270 nm for **FA**. TEM image of **GNP-FA-Glu** indicated that the average diameter of GNPs was 5 nm (Figure 2b). The size distribution of **GNP-FA-Glu** centered around 10 nm indicating that the GNPs were dispersed well (Figure S1).

3.2 Enhancement of cellular uptake of DLGNPs compared with mono-ligand GNPs

We quantitatively determined the cell binding and cellular uptake of GNPs in FR over-expressing KB cells. KB cells were treated with **GNP-FA** at different concentrations or incubated for different times. Figure 3a indicated that the cellular uptake of **GNP-FA** was saturated at 1 h after treatment with 10, 20 or 50 μg/mL GNPs. The cellular uptake amounts of **GNP-FA** were increased until 50 μg/mL. For experiments, we used a GNP concentration of 50 μg/mL and an incubation time of 2 h.

Figure 3b showed the cellular uptake of KB cells after treatment with 50 μg/mL GNPs for 2 h at 37 °C. As expected, **GNP-FA** showed more cellular uptake compared with **GNP-Glu**. The uptake of **GNP-FA-Glu** was increased by 3.9 folds compared with **GNP-FA** and by 12.7 folds compared with **GNP-Glu**. This enhancement was much more than an additive effect of **GNP-FA** and **GNP-Glu** suggesting a possible cooperative multivalent interaction. To prove this, we first treated KB cells with free FA, glucose, or both before adding **GNP-FA-Glu**. In all situations, the cell binding and cellular uptakes were effectively blocked indicating that the enhanced cell recognition was due to the cooperative binding of both ligands (Figure 3b).

Nanoparticles functionalized with targeting molecules usually enter cells through endocytosis.[32,33] The energy dependent endocytosis could be blocked at low temperature or in the presence of a metabolic inhibitor, such as NaN_3. To test the FA mediated endocytosis for cellular uptake of DLGNPs, KB cells were incubated with **GNP-FA-Glu** at 4 °C or in the presence of NaN_3 (0.2% w/v) at 37 °C (Figure S2). The gold content decreased dramatically at 4 °C or in the presence of NaN_3, indicating the internalization of DLGNPs is energy dependent, thus the receptor-mediated endocytosis is the predominant mechanism for GNP internalization [34].

3.3 Enahcenment of cellular uptake of DLGNPs for targeting cancer cells compared with non-targeting cancer cells

To explore the selectivity between targeting cancer cells and cells with low level of FR, A549 cells were investigated as a comparison to KB cells. The gold content in KB cells was only 4.1 folds more than that in A549 cells for **GNP-FA**, and almost equal for **GNP-Glu** in both cells (Figure 4). However, the gold content in KB cells was 11.8 folds more than that in A549 cells for **GNP-FA-Glu**. The results demonstrated quantitatively that **GNP-FA-GLu** conjugated with both FA and glucose could enhance the selectivity to FR over-expressing KB cells caused by multivalent interactions of GNPs with cells.

This conclusion was further supported by the CFM images and flow cytometry (Figure 5). A small amount of **TA-FITC** was incorporated into GNPs to allow the tracking of the particles inside cells. The interaction of fluorescent GNPs with KB cells was examined using fluorescence microscopy (Figure 5a). The highest levels of internalization were observed in KB cells incubated with **GNP-FA-Glu**, indicating FA/glucose dual-targeting approach enhanced the absolute amount of GNPs in cells with high FR expression. For A549 cells, no obvious internalization was observed for all kinds of GNPs (Figure 5a). For flow cytometry, the order of the fluorescence intensity in KB cells (Figure 5b) incubated with GNPs was **GNP-FA-Glu**>**GNP-FA**>**GNP-Glu**, which was consistent with cellular gold uptake results. No clear difference of fluorescence intensity was observed for A549 cells (Figure 5c).

3.4 Enhancement of selectivity of radiation-induced cell death by DLGNPs

Radiation can produce photoelectrons, auger electrons, or scattered photons, thereby damaging the targeted area via free radicals and ionization. Because the dose of ionizing radiation is proportional to the mass energy absorption coefficient of the media, localized GNPs can greatly increase the radiation dose received by cancer cells and tumor tissues.[35] The radiation mass energy absorption coefficient of gold is 2.074 $cm^2\ g^{-1}$, which is two orders of magnitude greater than that of soft tissue ($2.545\times10^{-2}\ cm^2\ g^{-1}$). We hypothesize that the DLGNPs with high cancer targeting efficiency should have the ability to enhance radiation-induced cell death selectivity.

To prove the hypothesis, we firstly optimized the radiation condition using KB cells and **GNP-FA**. The KB cells were incubated with GNP-FA at different conditions for 2 h and irradiated under X-rays at different kVs with same dose. After irradiation, cells were incubated for 48 h and then XTT assay was used to measure the surviving cell. The radiation response enhancements were observed for all conditions (Figure S3) [36]. X-ray at 100 kV induced more cytotoxicity than that at 50 kV. Finally, we selected 100 kV and a single dose of 10 Gy as the optimized X-ray parameters.

Figure 6 shows that irradiation (X-ray beam energy, 100 kV; loading dose, 10 Gy) induced cytotoxicity in KB cells. Before irradiation, GNPs had low toxicity in both KB and A549 cells. Therefore, the radiation-induced damage to the cancer cells was proportional to the quantity of X-ray absorbed by GNPs internalized by the cells. X-ray irradiation induced less

than 10% cell death without GNPs for both cells. Under X-ray irradiation, **GNP-FA** and **GNP-Glu** induced 40% and 20% cell death in KB cells respectively (Figure 6b), but only 10% cell death in A549 (Figure 6a). **GNP-FA-Glu** induced 80% cell death in KB cells compared with ~15% in A549 cells. For KB cells, the selectivity of **GNP-FA-Glu** was twice as that of **GNP-FA**, and four times as that of **GNP-Glu**. This order is the same as cellular uptake of these GNPs. The selectivity of GNP-FA-Glu was more than 5 times for KB cells than that for FR low-expressing A549 cells. The results demonstrated that DLGNPs with FA and glucose enhanced the radiation-induced cell death in FR over-expressing KB cells while showed low cytotoxicity to FR low-expressing A549 cells.

4. Conclusion

We designed and synthesized a dual-ligand cancer-targeting GNP containing both FA and glucose. The cancer cell recognition by the DLGNPs was significantly enhanced compared to mono-ligand GNPs. Furthermore, the internalization of DLGNPs was demonstrated to be mainly the dual-ligand-induce multivalent interaction with cells and endocytosis. Under X-ray irradiation, an enhancement of contrast between FR over-expressing cells and FR low-expressing cells (mimic of normal cells) was mediated by DLGNPs. These results strongly suggest that the multivalent interactions between DLGNPs and cancer cells play a key role in the enhancement of cell recognition and radiation-induced cell death. Such nanoparticles have great potential in CT imaging enhancement, targeted drug delivery, and radiotherapy enhancement.

Supplementary Material

Refer to Web version on PubMed Central for supplementary material.

Acknowledgments

We thank Sharon Frase, Thomas Mohaupt, Paul Thomas, Jennifer Peters and Samuel Connell for technical assiatance. This work was supported by National Cancer Institute (P30CA027165), the American Lebanese Syrian Associated Charities (ALSAC), the National Basic Research Program of China (973 Program 2010CB933504), and National Natural Science Foundation of China (21077068).

References

1. Hainfeld JF, Slatkin DN, Smilowitz HM. The use of gold nanoparticles to enhance radiotherapy in mice. Phys Med Biol 2004;49(18):309–315.
2. Morris KN, Weil MD, Malzbender R. Radiochromic film dosimetry of contrast-enhanced radiotherapy (CERT). Phys Med Biol 2006;51(22):5915–25. [PubMed: 17068373]
3. Hainfeld JF, Dilmanian FA, Slatkin DN, Smilowitz HM. Radiotherapy enhancement with gold nanoparticles. J Pharm Pharmacol 2008;60(8):977–85. [PubMed: 18644191]
4. Pignol JP, Rakovitch E, Beachey D, Le Sech C. Clinical significance of atomic inner shell ionization (ISI) and Auger cascade for radiosensitization using IUdR, BUdR, platinum salts, or gadolinium porphyrin compounds. Int J Radiat Oncol Biol Phys 2003;55(4):1082–91. [PubMed: 12605988]
5. Corde S, Joubert A, Adam JF, Charvet AM, Le Bas JF, Esteve F, et al. Synchrotron radiation-based experimental determination of the optimal energy for cell radiotoxicity enhancement following photoelectric effect on stable iodinated compounds. Br J Cancer 2004;91(3):544–51. [PubMed: 15266326]
6. Pennington JA. A review of iodine toxicity reports. J Am Diet Assoc 1990;90(11):1571–81. [PubMed: 2229854]
7. Sherer TT, Thrall KD, Bull RJ. Comparison of toxicity induced by iodine and iodide in male and female rats. J Toxicol Environ Health 1991;32(1):89–101. [PubMed: 1987365]

8. Lorberboym M, Mechanick JI. Accelerated thyrotoxicosis induced by iodinated contrast media in metastatic differentiated thyroid carcinoma. J Nucl Med 1996;37(9):1532–5. [PubMed: 8790212]
9. Haller C, Schick CS, Zorn M, Kubler W. Cytotoxicity of radiocontrast agents on polarized renal epithelial cell monolayers. Cardiovasc Res 1997;33(3):655–65. [PubMed: 9093536]
10. Ross JF, Chaudhuri PK, Ratnam M. Differential regulation of folate receptor isoforms in normal and malignant tissues in vivo and in established cell lines-physiological and clinical implications. Cancer 1994;73(9):2432–43. [PubMed: 7513252]
11. Cho SH. Estimation of tumour dose enhancement due to gold nanoparticles during typical radiation treatments: a preliminary Monte Carlo study. Phys Med Biol 2005;50(15):163–73.
12. De Jong WH, Hagens WI, Krystek P, Burger MC, Sips A, Geertsma RE. Particle size-dependent organ distribution of gold nanoparticles after intravenous administration. Biomaterials 2008;29(12):1912–9. [PubMed: 18242692]
13. Semmler-Behnke M, Kreyling WG, Lipka J, Fertsch S, Wenk A, Takenaka S, et al. Biodistribution of 1.4-and 18-nm gold particles in rats. Small 2008;4(12):2108–11. [PubMed: 19031432]
14. Sonavane G, Tomoda K, Makino K. Biodistribution of colloidal gold nanoparticles after intravenous administration: Effect of particle size. Colloid Surf B Biointerfaces 2008;66(2):274–80.
15. Torchilin V. Antibody-modified liposomes for cancer chemotherapy. Expert Opin Drug Deliv 2008;5(9):1003–25. [PubMed: 18754750]
16. Arruebo M, Valladares M, Gonzalez-Fernandez A. Antibody-conjugated nanoparticles for biomedical applications. J Nanomater 2009:489389.
17. Keefe AD, Pai S, Ellington A. Aptamers as therapeutics. Nat Rev Drug Discov 2010;9(7):537–50. [PubMed: 20592747]
18. Lee JH, Yigit MV, Mazumdar D, Lu Y. Molecular diagnostic and drug delivery agents based on aptamer-nanomaterial conjugates. Adv Drug Deliv Rev 2010;62(6):592–605. [PubMed: 20338204]
19. Ray P, White R. Aptamers for targeted drug delivery. Pharmaceuticals 2010;3:1761–78.
20. Lee S, Xie J, Chen XY. Peptide-based probes for targeted molecular imaging. Biochemistry 2010;49(7):1364–76. [PubMed: 20102226]
21. Pangburn TO, Petersen MA, Waybrant B, Adil MM, Kokkoli E. Peptide- and aptamer-functionalized nanovectors for targeted delivery of therapeutics. J Biomech Eng 2009;131(7): 074005. [PubMed: 19655996]
22. Blondin C, Bataille I, Letourneur D. Polysaccharides for vascular cell targeting. Crit Rev Ther Drug Carrier Syst 2000;17(4):327–75. [PubMed: 10958246]
23. Lemarchand C, Gref R, Couvreur P. Polysaccharide-decorated nanoparticles. Eur J Pharm Biopharm 2004;58(2):327–41. [PubMed: 15296959]
24. Quintana A, Raczka E, Piehler L, Lee I, Myc A, Majoros I, et al. Design and function of a dendrimer-based therapeutic nanodevice targeted to tumor cells through the folate receptor. Pharm Res 2002;19(9):1310–6. [PubMed: 12403067]
25. Kukowska-Latallo JF, Candido KA, Cao ZY, Nigavekar SS, Majoros IJ, Thomas TP, et al. Nanoparticle targeting of anticancer drug improves therapeutic response in animal model of human epithelial cancer. Cancer Res 2005;65(12):5317–24. [PubMed: 15958579]
26. Liong M, Lu J, Kovochich M, Xia T, Ruehm SG, Nel AE, et al. Multifunctional inorganic nanoparticles for imaging, targeting, and drug delivery. Acs Nano 2008;2(5):889–96. [PubMed: 19206485]
27. Weitman SD, Lark RH, Coney LR, Fort DW, Frasca V, Zurawski VR, et al. Distribution of the folater receptor GP38 in normal and malignant cell lines and tissues. Cancer Res 1992;52(12): 3396–401. [PubMed: 1596899]
28. Jimeno A, Hidalgo M. Multitargeted therapy: Can promiscuity be praised in an era of political correctness? Crit Rev Oncol Hematol 2006;59(2):150–8. [PubMed: 16843676]
29. Saul JM, Annapragada AV, Bellamkonda RV. A dual-ligand approach for enhancing targeting selectivity of therapeutic nanocarriers. J Control Release 2006;114(3):277–87. [PubMed: 16904220]

30. Ying X, Wen H, Lu WL, Du J, Guo J, Tian W, et al. Dual-targeting daunorubicin liposomes improve the therapeutic efficacy of brain glioma in animals. J Control Release 2010;141(2):183–92. [PubMed: 19799948]

31. Kluza E, van der Schaft DWJ, Hautvast PAI, Mulder WJM, Mayo KH, Griffioen AW, et al. Synergistic targeting of alpha(v)beta(3) integrin and galectin-1 with heteromultivalent paramagnetic liposomes for combined MR imaging and treatment of angiogenesis. Nano Lett 2010;10(1):52–8. [PubMed: 19968235]

32. Kam NWS, Liu ZA, Dai HJ. Carbon nanotubes as intracellular transporters for proteins and DNA: An investigation of the uptake mechanism and pathway. Angew Chem Int Ed 2006;45(4):577–81.

33. Chen JY, Chen SY, Zhao XR, Kuznetsova LV, Wong SS, Ojima I. Functionalized single-walled carbon nanotubes as rationally designed vehicles for tumor-targeted drug delivery. J Am Chem Soc 2008;130(49):16778–85. [PubMed: 19554734]

34. Silverstein SC, Steinman RM, Cohn ZA. Endocytosis. Annu Rev Biochem 1977;46:669–722. [PubMed: 332066]

35. Kong T, Zeng J, Wang XP, Yang XY, Yang J, McQuarrie S, et al. Enhancement of radiation cytotoxicity in breast-cancer cells by localized attachment of gold nanoparticles. Small 2008;4(9):1537–43. [PubMed: 18712753]

36. Liu CJ, Wang CH, Chen ST, Chen HH, Leng WH, Chien CC, et al. Enhancement of cell radiation sensitivity by pegylated gold nanoparticles. Phys Med Biol 2010;55(4):931–45. [PubMed: 20090183]

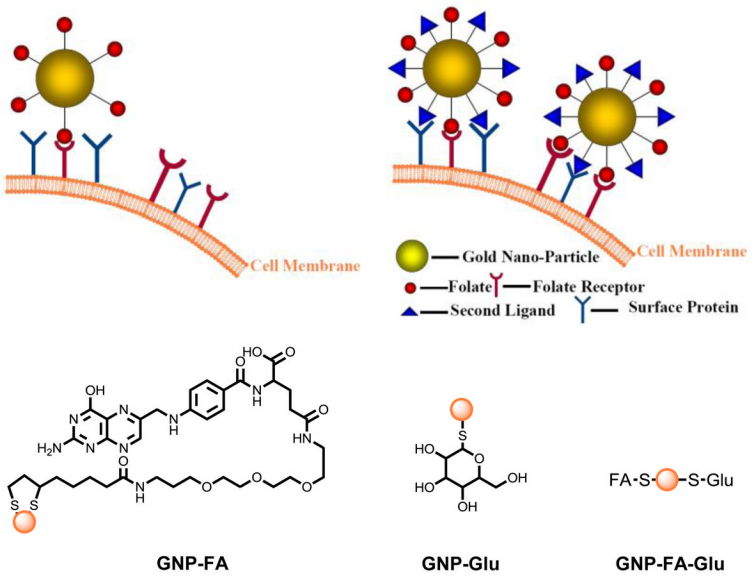

Figure 1.
Schematic representation of synthesis of GNPs and their interaction with cancer cells through multivalent interactions.

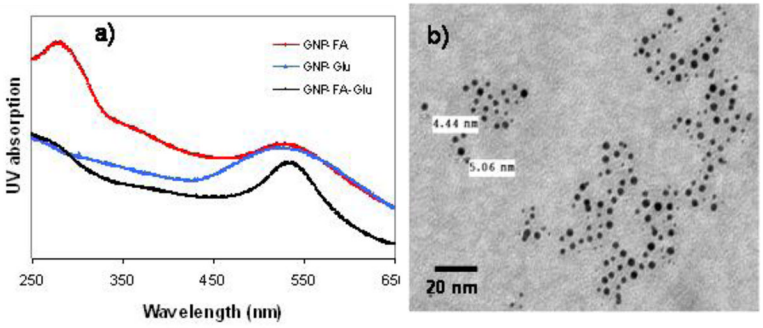

Figure 2.
(a) UV-Vis absorption spectra of GNPs and (b) TEM image of **GNP-FA-Glu**. The scale bar is 20 nm.

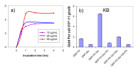

Figure 3.
(a) Optimization of incubation time and gold concentration of KB cells for GNP-FA, and (b) cellular uptake of KB cells for different GNPs under different conditions. The gold concentration is 50 μg/mL. The gold concentrations in cells were determined by ICP-MS. The data represent the mean ± standard deviation of the results from three experiments.

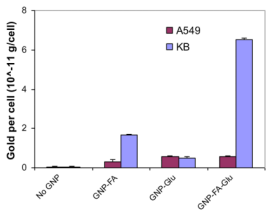

Figure 4.

Cellular uptake of GNPs for FR over-expressing KB cells and FR low-expressing A549 cells. The data represent the mean ± standard deviation of the results from three experiments.

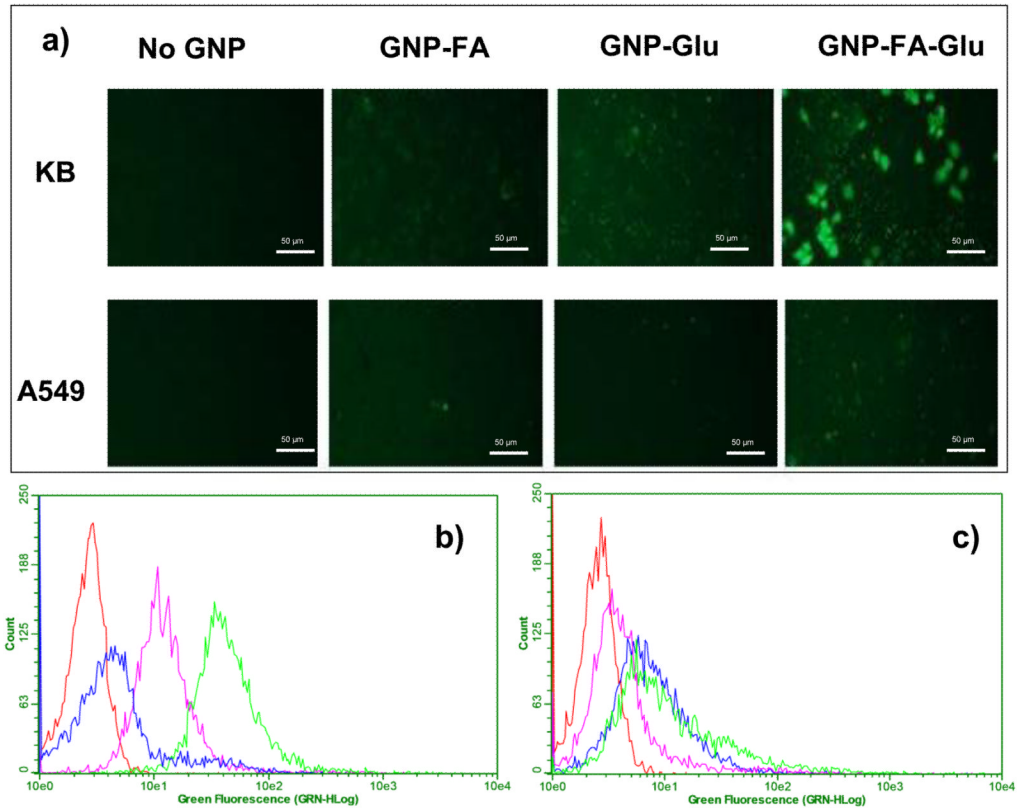

Figure 5.

(a) Confocal fluorescence microscopy (CFM) images of KB and A549 cells after treated with different GNPs. All GNPs were labeled with **TA-FITC** which had green fluorescence. The scale bar is 50 μm. Flow cytometry assay to monitor the binding of GNPs with (b) KB and (c) A549 cells. The red, blue, pink and green curves represented cell control, cells treated with **GNP-Glu**, **GNP-FA** and **GNP-FA-Glu**, respectively.

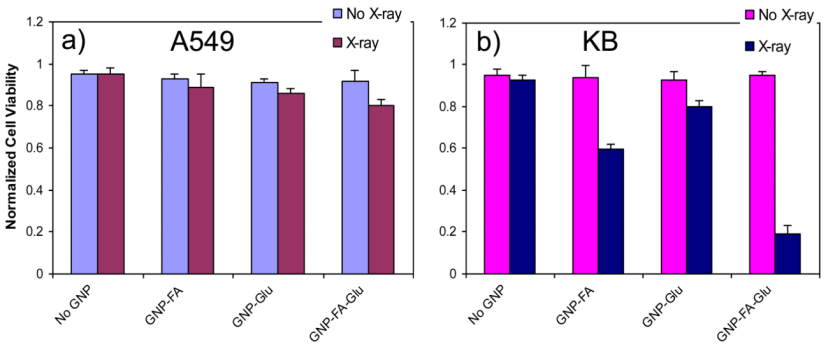

Figure 6.

Cell viability of (a) A549 and (b) KB cells incubated with GNPs under X-ray irradiation. The X-ray experiments were performed using the Minishot X-ray cabinet at 100 kV for a single dose of 10 Gy. The data represent the mean ± standard deviation of the results from three experiments.